

Electron-electron interactions and the phase diagram of a graphene bilayer

Johan Nilsson,¹ A. H. Castro Neto,¹ N. M. R. Peres,² and F. Guinea³¹Department of Physics, Boston University, 590 Commonwealth Avenue, Boston, MA 02215, USA²Center of Physics and Departamento de Física,
Universidade do Minho, P-4710-057, Braga, Portugal³Instituto de Ciencia de Materiales de Madrid, CSIC, Cantoblanco E28049 Madrid, Spain
(Dated: April 28, 2006)

We study the effects of long and short-range electron-electron interactions in a graphene bilayer. Using a variational wavefunction technique we show that in the presence of long-range Coulomb interactions the clean bilayer is always unstable to electron and hole pocket formation with a finite ferromagnetic polarization. Furthermore, we argue that short-range electron-electron interactions lead to a staggered orientation of the ordered ferromagnetic moment in each layer (that is, c-axis antiferromagnetism). We also comment on the effects of doping and trigonal distortions of the electronic bands.

PACS numbers: 71.10.-w, 75.10.Lp, 75.70.Ak, 71.70.Gm

I. INTRODUCTION

The recent developments in the field of carbon physics, where a few layers or even single layers of graphene have been isolated, have shown that the physics of these systems is unconventional from the point of view of traditional semiconductor and Fermi-liquid physics^{1,2}. The electronic dispersion of graphene close to the two K-points of the Brillouin zone can be written as³: $E(\mathbf{p}) = v_F |\mathbf{p}|$, where v_F is Dirac-Fermi velocity (this expression is valid for two-dimensional momentum $\mathbf{p} = (p_x, p_y)$ such that $|\mathbf{p}| < \hbar/a$ where a is a momentum cut-off of the order of the inverse of the lattice spacing a). This dispersion relation is identical to the one of Dirac electrons with "speed of light" given by v_F . In this case the electron effective mass, m^* , is zero, and the density of states vanishes at the K-point. The vanishing of the effective mass, the interplay of interactions, disorder, and extended defects, lead to anomalous behavior in many physical properties^{4,5}.

The capability of experimentally controlling the number of graphene layers opens up the field for the study of the effect of interlayer coupling in a strongly interacting two-dimensional system. Interlayer coupling is a controversial topic in the graphite literature where the precise nature of the coupling between graphene planes is unsettled^{6,7}. Another important issue in carbon research has to do with the weak ferromagnetism in highly disordered graphite that have been observed in experiments⁸ but is still a theoretically open problem^{9,10}.

It is well-known that the low-density electron gas with long-range Coulomb interactions in two and three dimensions is unstable toward a ferromagnetic state. The original argument due to Bloch relies on a variational calculation of the ground state energy¹¹. Recently this approach was used to look for a possible ferromagnetic instability in a single layer of graphene¹⁰. The parameter that controls the relative strength between kinetic and Coulomb energies is the dimensionless coupling, $g = e^2/\epsilon_0 v_F$; ($\hbar = 1$) where e is the electric charge ($e^2 = 14.4$ eV Å),

and ϵ_0 is the graphene dielectric constant ($\epsilon_0 = 1$). In that case, ferromagnetism is only found for values of g larger than a critical value, $g_c = 5.3$, which is larger than its estimated value in graphene ($g = 2.1$). An analysis based on short-range interactions seems to confirm this picture⁵.

In this paper we use a similar variational technique to study a clean graphene bilayer where we include the hopping between graphene planes. Unlike the case of a single layer, we find that the bilayer is always unstable toward a ferromagnetic state with formation of electron and hole pockets with a polarization of the order of 10^{-6} to 10^{-5} electrons per carbon. This result may have direct implications for the interpretation of the magneto-transport data in graphitic devices¹².

The paper is organized as follows: In Section II the model is introduced. In Section III we explain the variational calculation and present the phase diagram. The influence of other hopping parameters on the instability are discussed in Section IV. Section V includes the results for the low-energy susceptibilities and a discussion of short range interactions. The conclusions of the paper are to be found in Section VI. We also include appendices with some mathematical details.

II. THE MODEL

The lattice structure for the bilayer which is just one unit cell of graphite is depicted in Fig. 1. For simplicity we model the system by the nearest neighbor tight-binding Hamiltonian:

$$H_{t.b.} = \sum_{\langle m, n \rangle} t \sum_{i,j} (c_{A_1, m}^\dagger c_{B_1, n} + h.c.) + \sum_{\langle m, n \rangle} t_2 \sum_{i,j} (c_{A_1, m}^\dagger c_{A_2, n} + h.c.); \quad (1)$$

where $c_{a_i, m}$; ($c_{a_i, m}^\dagger$) annihilates (creates) an electron on site m of the sublattice a ($a = A; B$) of plane i

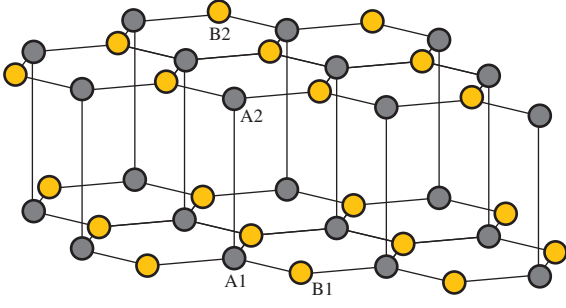


FIG. 1: (Color online) Lattice structure of the bilayer. The A-sublattices are indicated by the darker spheres.

($i = 1; 2$), with spin ($\sigma = \uparrow; \downarrow$), t ($t \approx 3$ eV) is the in-plane hopping energy and t_\perp ($t_\perp \approx 0.35$ eV in graphite⁶) is the hopping energy between atom A_1 and atom A_2 (see Fig. 1). A similar tight-binding Hamiltonian for graphite and the single graphene layer was studied long ago by Wallace³. At low energies and long wavelengths, the kinetic Hamiltonian can be expanded around the K (K') points in the Brillouin zone. The resulting Hamiltonian can be written as:

$$H_{\text{kin}} = \sum_{\mathbf{p}} \sum_{i,j,a} \sum_{\sigma} \psi_{\mathbf{p};i,j,a;\sigma}^\dagger K(\mathbf{p})_{ij} \psi_{\mathbf{p};j,i,a;\sigma} \quad (2)$$

with $\psi_{\mathbf{p};i,j,a;\sigma}$ denoting $\psi_{\mathbf{p};i,j,a;\sigma}$ and $\sum_{\mathbf{p}} = \sum_{\mathbf{p}} (c_{\mathbf{p};iA_1;\sigma}^\dagger; c_{\mathbf{p};iB_1;\sigma}^\dagger; c_{\mathbf{p};iA_2;\sigma}^\dagger; c_{\mathbf{p};iB_2;\sigma}^\dagger)$. Here, $c_{\mathbf{p};i,j,a;\sigma}^\dagger$ ($c_{\mathbf{p};i,j,a;\sigma}$) creates (annihilates) an electron with momentum \mathbf{p} , on sublattice i ($i = A; B$) of plane j ($j = 1; 2$), with spin ($\sigma = \uparrow; \downarrow$) at the K-point a ($a = 1; 2$) in the Brillouin zone, and

$$K(\mathbf{p}) = \begin{pmatrix} 0 & 0 & p e^{i(\mathbf{p})} & t_\perp \\ p e^{i(\mathbf{p})} & 0 & 0 & 0 \\ t_\perp & 0 & 0 & p e^{i(\mathbf{p})} \\ 0 & 0 & p e^{i(\mathbf{p})} & 0 \end{pmatrix} \quad (3)$$

is the kinetic energy matrix where $p = \tan^{-1}(p_y/p_x)$. We have set $v_F = 1 = \hbar$, so that the energy is measured in units of the in-plane hopping, t , and distance is measured in units of carbon-carbon distance a ($a \approx 1.42$ Å)⁶.

The kinetic term can be diagonalized by a unitary transformation: $\psi = M_p \phi$, where M_p is given in Appendix A. Then $H_{\text{kin}} = \sum_{\mathbf{p};j,i,a} E_j(\mathbf{p}) \sum_{\mathbf{p};j,i,a} \phi_{\mathbf{p};j,i,a}^\dagger \phi_{\mathbf{p};j,i,a}$, where the four energy bands are given by:

$$\begin{aligned} E_1(\mathbf{p}) &= t_\perp/2 + E(\mathbf{p}); \\ E_2(\mathbf{p}) &= t_\perp/2 - E(\mathbf{p}); \\ E_3(\mathbf{p}) &= t_\perp/2 + E(\mathbf{p}); \\ E_4(\mathbf{p}) &= t_\perp/2 - E(\mathbf{p}); \end{aligned}$$

where $E(\mathbf{p}) = \sqrt{p^2 + t_\perp^2/4}$. The bands are sketched in Fig. 2. Any state of the system can be labeled in terms of the occupation of each band, $n_{i,j,a}(\mathbf{p})$, with

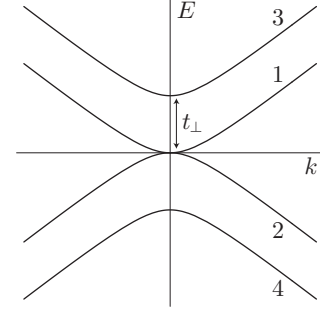


FIG. 2: Band dispersions near the K-points in the bilayer. Bands are labeled by the numbers 1–4 as in the text.

$i = 1; 2; 3; 4$. The non-interacting ground state has degeneracy 4 per momentum, per plane, due to the SU(2) spin rotation symmetry and the Z_2 real space sublattice exchange symmetry (at low energies this symmetry becomes SU(2) for the continuous rotation of the K and K' states in momentum space), and occupation at half-filling, given by: $n_{1,j,a}(\mathbf{p}) = 0$, $n_{2,j,a}(\mathbf{p}) = 1$, $n_{3,j,a}(\mathbf{p}) = 0$ and $n_{4,j,a}(\mathbf{p}) = 1$. Hence, the presence of t_\perp does not mix the spins or the K-points. However, the two Dirac cones transform into vertex touching hyperbolae, and for $p \gg t_\perp$ the electrons acquire an effective mass, $m = t_\perp/2$.

The Coulomb interaction in the bilayer is conveniently written in terms of the Fourier components of symmetric and anti-symmetric combinations of the layer densities, $\rho_i(\mathbf{q}) = \rho_1(\mathbf{q}) \pm \rho_2(\mathbf{q})$, where $\rho_i(\mathbf{q}) = \sum_{\mathbf{k};j,i,a} c_{\mathbf{k}+\mathbf{q};j,i,a}^\dagger c_{\mathbf{k};j,i,a}$. The Coulomb term reads:

$$H_I = \frac{1}{2S} \sum_{\mathbf{q} \neq 0} \sum_{i,j,a} \rho_i(\mathbf{q}) V(\mathbf{q}) \rho_i(-\mathbf{q}) \quad (4)$$

where $V(\mathbf{q}) = 2\epsilon^2(1 - e^{i\mathbf{q} \cdot \mathbf{d}})/2_0q$, S is the area of the system, and d is the interplane distance ($d \approx 2.4a \approx 3.35A$, $d \approx 3.7$). We are going to show that in the presence of Eq. (4) the non-interacting ground state is unstable. To perform the calculation it is convenient to express the density operators in the diagonal basis: $\rho_i(\mathbf{q}) = \sum_{\mathbf{p};j,i,a} \phi_{\mathbf{p}+\mathbf{q};j,i,a}^\dagger \phi_{\mathbf{p};j,i,a}$ and write the exchange energy associated with Eq. (4) as:

$$\frac{E_{\text{ex}}}{S} = \frac{1}{2} \sum_{\mathbf{p}} \frac{d\mathbf{p}}{(2\pi)^2} \frac{d^2\mathbf{p}^0}{(2\pi)^2} \sum_{i,j,a} \phi_{ij}^0(\mathbf{p}) \phi_{ji}^0(\mathbf{p}) n_{i,j,a}(\mathbf{p}^0) n_{j,i,a}(\mathbf{p}) V(\mathbf{p}^0 - \mathbf{p}) \quad (5)$$

The definitions of the matrices and some more details about the exchange interaction for Bloch electrons and Eq. (5) are given in Appendix B.

III. VARIATIONAL CALCULATION AND PHASE DIAGRAM

Consider the half-filled case with a variational state with one electron pocket in the spin up channel and one hole pocket in the spin down channel at each K-point: $n_{1,\uparrow;a}(p) = (Q - p)$, $n_{1,\downarrow;a}(p) = 0$, $n_{2,\uparrow;a}(p) = 1$, and $n_{2,\downarrow;a}(p) = 1 - (Q - p)$, where Q , the size of the pocket, is a variational parameter (in what follows we assume $Q < t_z$ and hence the occupations of bands 3 and 4 are not affected). Pictures of the non-interacting ground state and the trial state are shown in Fig. 3a and 3b. Notice that the size of the pocket is the same in different channels because of the conservation of the number of electrons at half-filling. This state breaks the $SU(2)$, but not the Z_2 symmetry, and is therefore spin polarized (ferromagnetic). There is a similar state that breaks both symmetries and has no net magnetization: an electron (hole) pocket in the up (down) spin channel in K-point 1 and a hole (electron) pocket in the up (down) channel in K-point 2. We can show that the spin polarized state is lower in energy (see below).

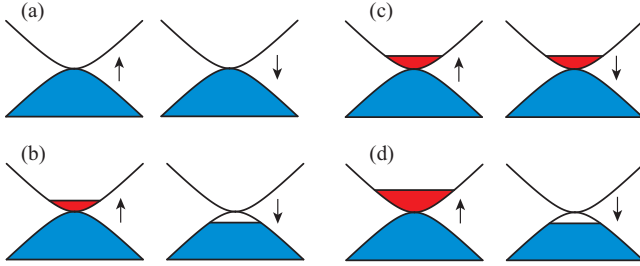


FIG. 3: (Color online) Sketch of the trial states: (a) Half-filled non-interacting ground state, (b) Trial state with particle-hole pockets built upon (a), (c) Doped non-interacting ground state, (d) Trial state with particle-hole pockets built upon (c).

The change in the kinetic energy per unit area due to an electron (or hole) pocket of size Q is given by:

$$\frac{E_{\text{kin}}}{S} = \frac{1}{2} \frac{(Q^2 + t_z^2 = 4)^{3/2}}{3} - \frac{t_z^3}{24} - \frac{t_z Q^2}{4} - \frac{Q^4}{8 t_z}; \quad (6)$$

up to order Q^4 . The expressions for the change in the exchange energy are cumbersome and details are provided in Appendix C. We end from Eq. 5), up to the same order:

$$\frac{E_{\text{ex}}(Q)}{S} = \frac{g}{8 t_z^2} \frac{8}{27} Q^3 + \frac{h}{4} \frac{3}{8} + \frac{1}{2} \ln(4=t_z) - \frac{1}{4} \int_0^{t_z} \frac{e^{-dy}}{t_z^2 = 4 + y^2} \frac{1}{t_z} Q^4 : \quad (7)$$

Notice that the leading order term in the exchange interaction is $E_{\text{ex}} = S \frac{gQ^3}{27 t_z^2} \sim m^{3/2}$, where m is the magnetization, which is always dominant over

the kinetic term that is of order $Q^4 \sim m^2$. Therefore, we have proved that the bilayer is always unstable to the formation of polarized electron and hole pockets. In contrast to the single graphene plane case¹⁰, the total energy is negative for small Q . This is due to the fact that the exchange with the filled bands is less important in this case. In order to calculate the equilibrium size of the pockets we minimize the total energy,

$E_{\text{tot}}(Q) = E_{\text{kin}}(Q) + E_{\text{ex}}(Q)$, with respect to Q and Q_{min} , that is, the size of the pocket for which the energy is minimized. For the parameters in graphene (see below) we find that $Q_{\text{min}} \approx 0.05 t_z$ (t_z), justifying the above expansion.

Consider the case where the system is initially doped with pockets of size Q_0 ($n = Q_0^2 = 2$). We look for an instability by varying the density of electrons and holes subject to the constraint of particle conservation. Note that the instability can produce one type of carrier (either electron or hole) if $Q_0 > Q_{\text{min}}$ or two type of carriers (electrons and holes) if $Q_0 < Q_{\text{min}}$. We can parameterize the state with one type of carrier by taking $Q_{\uparrow}^2 = Q_0^2 (2 - x)$ and $Q_{\downarrow}^2 = Q_0^2 x$ with $0 \leq x \leq 1$. For the state with two types of carriers we take instead $Q_{\uparrow}^2 = 2Q_0^2 + \mathbf{x} \cdot \mathbf{j}$ and $Q_{\downarrow}^2 = \mathbf{x} \cdot \mathbf{j}$, with $x \leq 0$. The doped non-interacting ground state and the trial state with particle-hole pockets ($x < 0$) are shown pictorially in Fig. 3c and 3d. The calculation proceeds as before and we find:

$$\frac{E}{S} = \frac{1}{2S} [E_{\text{tot}}(Q_{\uparrow}) + E_{\text{tot}}(Q_{\downarrow}) - 2E_{\text{tot}}(Q_0)] + E_{\text{extra}}(Q_0; \mathbf{x}): \quad (8)$$

The extra term, $E_{\text{extra}}(Q_0; \mathbf{x})$, comes from terms that cancel out in the undoped case. To leading order in Q these terms are given by $gQ_0^4(1 - x)^2 = (64)$ for $x = 0$ and $gQ_0^2(Q_0^2 + 2\mathbf{x} \cdot \mathbf{j}) = (64)$ when $x = 0$. In our units we have $t_z = 1$ so that, to a first approximation, this contribution is much smaller than the quartic term in Eq. (7), and it can be neglected. This leaves us with the first line in Eq. (8) involving E_{tot} only. The dependence on x is implicit through Q_{\uparrow} and Q_{\downarrow} . Then Eq. (8) has the form:

$E(Q) = A \mathcal{Q}^3 + B \mathcal{Q}^4$. Rescaling the Q variable so that the minimum of the energy in the paramagnetic states sits at $\mathcal{Q} = 1$, we have:

$$E(Q) = \mathcal{Q}^3 + \mathcal{Q}^4: \quad (9)$$

Using the scaled variables we see that the system is unstable to small deviations in x from 1 if $Q_0 = 1 = 2$. The ferromagnetic state has lower energy than the paramagnetic states if $Q_0 < 0.7$ and the resulting state has electron and hole pockets. As a consequence of the first order nature of the transition, the system exhibits phase coexistence (that can be obtained from a Maxwell construction, not shown in the Fig. 4), and hysteresis in physical properties such as magneto-transport, around the critical line. In this region, the system shows a tendency towards electronic phase separation¹³, frustrated by electrostatic effects. As the charge densities involved

are rather low (see below) we cannot exclude the formation of large domains of the different phases. The phase diagram for $t_2 = 0.05$ is shown in Fig. 4 as well as a plot of $E(Q_0; x)$ for some typical cases of Q_0 .

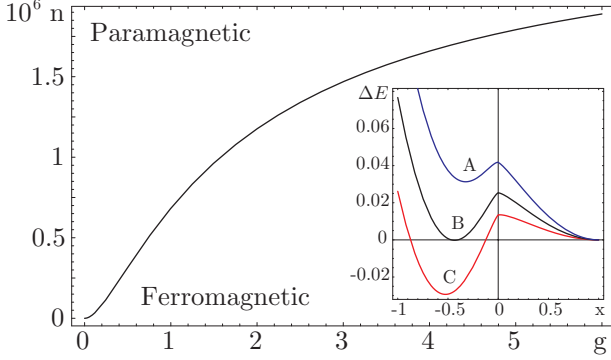


FIG. 4: (Color online) Left: Phase diagram of the graphene bilayer as a function of electron density away from half-filling, n (electrons per carbon), and coupling strength, $g = e^2/(v_F t_2)$, with $t_2 = 0.05$. Inset: E as a function of x (as defined in the text) in the paramagnetic (A), and ferromagnetic (C) regions of the phase diagram.

In the previous calculation we have not included the exchange interaction between different K -points in the Brillouin zone. In that case the spin polarized state that breaks $SU(2)$ is degenerate with the state that breaks both $SU(2)$ and Z_2 . The difference between the states is how the pockets are assigned to the spins and the K -points. By including exchange between K -points in Eq. (5) we find that there is small energy difference between the states favoring a state with a net ferromagnetism but which retains the Z_2 symmetry. Quite generally this is the case since the elements of $\epsilon_{ij}(p^0; p)_{ji}(p; p^0)$ are all positive. A direct calculation using Eq. (5) and taking p and p^0 to lie at nearest neighboring K -points confirms this picture. One then finds a very small energy difference of order $1/Q^4$, and hence other effects can be important in determining the actual ground state. There is also a correction to the $Q^4 t_2$ -term in Eq. (7) that changes the position of the optimal value of Q_{min} by a small amount.

In order to compare with experiments it is interesting to estimate the total magnetization in the polarized state for the case of the undoped graphene bilayer. We estimate the cut-off using a Debye approximation so the number of states is conserved in the Brillouin zone: $2 = 2 \Rightarrow A_u = 4 = (27a^2)$, where A_u is the area of the real space unit cell. Restoring the units, we set $v_F = 3 \times 10^6$ m/s, and $t_2 = 1/(v_F) \approx 5.2 \times 10^{-2}$, where $1 \approx 0.37$ eV is the typical graphite value⁶. Hence, for two pockets of size Q the density of electrons per carbon is approximately $n = Q^2/4 \approx 1.6 \times 10^6$ ($t_2 = 0.05$ and $Q \approx 0.05 t_2$), and therefore, the magnetization per carbon is $m \approx 10^6 / 10^5 B$ (B is the Bohr magneton). These numbers are, of course, very approximate because the value of the microscopic parameters do not need to be

the same as in graphite and the presence of a cut-off introduces further uncertainty. In any event, the magnetized state of the graphene bilayer shows very weak ferromagnetism. A direct experimental consequence of our calculation is that the bilayer has two species of electrons (electrons and holes) and therefore they should contribute to the Hall resistivity at small magnetic fields, B . In particular, it is easy to show that the magnetoresistance at small magnetic fields acquires a B^2 dependence¹⁴.

IV. OTHER HOPPING PARAMETERS

We would like to comment on other effects that we have not considered in the previous calculation. In terms of the Slonczewski-Weiss-McClure model for graphite^{15,16} our model includes only the parameters $t_0(t)$ and $t_1(t_2)$ but not t_3 and t_4 . On the one hand, t_4 introduces an electron-hole asymmetry by changing the curvature of the bands, but the bands remain parabolic near half-filling. On the other hand, t_3 introduces a trigonal distortion which restores a linear dispersion at low energies. To estimate the effects of t_3 we use the effective low-energy model that can be derived from the extension of Eq. (3) to include t_3 and projecting onto the two bands that are closest to the Fermi surface (see Ref. [17] and Appendix E for details). The effective kinetic energy matrix is then:

$$K(p) = \frac{p^2}{t_2} \begin{pmatrix} 0 & e^{i2} \\ e^{i2} & 0 \end{pmatrix} + v_3 p \begin{pmatrix} 0 & e^i \\ e^i & 0 \end{pmatrix}; \quad (10)$$

where $v_3 = t_3/t_0$, with energy eigenvalues given by:

$$E(p) = \frac{p}{p^2 + (v_3 t_2)^2 + 2pv_3 t_2 \cos(3\theta)} t_2; \quad (11)$$

It is easy to see that the crossover from linear to quadratic dispersion takes place at a momentum $p_{cross} \approx v_3 t_2$. If $p_{cross} \ll Q_{min}$ ($v_3 \ll 0.1$) the previous calculation is still valid since the dispersion remains parabolic at the scale of the instability. Nevertheless, if one uses the values of the parameters in the graphite literature⁶, namely, $v_3 = t_3/t_0 \approx 0.1$ we conclude that $p_{cross} \approx Q_{min}$ and the trigonal distortion may become important. We should remark, once again, that it is not guaranteed that the value of the parameters in graphite are the same as in the bilayer (hence, one should take the numbers here with a grain of salt). At small energies, the spectrum in Eq. (10) can be described in terms of one Dirac cone at $p = 0$, and three asymmetric cones at $p_{cone} = v_3 t_2$ (the direction of the cones are such that $\cos(3\theta) = -1$). This situation maps onto the single graphene plane case¹⁰ with ellipsoidal pockets instead of circular, and a small renormalized Fermi velocity, $v_F = v_3 v_F$ (v_F). Therefore the dimensionless coupling strength is $g = g/v_3 \approx 20$, which is much larger than the critical coupling for ferromagnetism¹⁰. Then, in this case the transition from paramagnetism is into a fully polarized state with effective bandwidth of order of $v_3 t_2$, leading to a polarization

of the order of 10^{-6} electrons per carbon, which is of the same order of magnitude of polarization found without χ_3 . Unfortunately this argument is not rigorous since the exchange with the filled bands also contributes, requiring a more detailed study.

V. SHORT RANGE INTERACTIONS

We consider the effects of short-range electron-electron interactions which, for simplicity, we describe by an on-site Hubbard interaction, U . It turns out that this interaction favors an antiferromagnetic ordering. In order to quantify the tendency towards this phase, we calculate the associated susceptibility and present a simple mean field argument.

A. Electronic susceptibility.

Using the basis defined in Eq. (10) with $v_3 = 0$ (the procedure outlined in Appendix E) the wavefunctions corresponding to the two bands closest to the Fermi level can be written approximately as:

$$\psi_{\pm}(\mathbf{k}) = \frac{1}{\sqrt{2}} \begin{pmatrix} e^{i\mathbf{k} \cdot \mathbf{r}_1} \\ e^{\pm i\mathbf{k} \cdot \mathbf{r}_2} \end{pmatrix}; \quad (12)$$

so that the states are mostly localized at the sites without a corresponding atom in the neighboring layer. Formally, this two component wavefunction is equivalent to

the spinor defined in the analysis of a single graphene plane except that the angle is doubled. Restricting the calculation to this subspace, we can write the bare susceptibility as a 2×2 matrix (Ref.18):

$$\chi_0(\mathbf{q};!) = \begin{pmatrix} \chi_D(\mathbf{q};!) & \chi_{ND}(\mathbf{q};!) \\ \chi_{ND}(\mathbf{q};!) & \chi_D(\mathbf{q};!) \end{pmatrix}; \quad (13)$$

Here χ_D denotes the response in the same plane as the source and χ_{ND} response in the opposite plane. The random phase approximation (RPA) susceptibility, assuming an on-site Hubbard interaction U , is:

$$\chi_{\text{RPA}}(\mathbf{q};!) = [\chi_0(\mathbf{q};!) - U \chi_0(\mathbf{q};!)]^{-1}; \quad (14)$$

This expression becomes simpler when decomposed into a contribution symmetric in the two sublattices and another antisymmetric:

$$\begin{aligned} \frac{\chi_{\text{FM}}(\mathbf{q};!)}{4} &= \frac{\chi_D(\mathbf{q};!) + \chi_{ND}(\mathbf{q};!)}{1 - U[\chi_D(\mathbf{q};!) + \chi_{ND}(\mathbf{q};!)]}; \\ \frac{\chi_{\text{AFM}}(\mathbf{q};!)}{4} &= \frac{\chi_D(\mathbf{q};!) - \chi_{ND}(\mathbf{q};!)}{1 - U[\chi_D(\mathbf{q};!) - \chi_{ND}(\mathbf{q};!)]}; \end{aligned} \quad (15)$$

The symmetric susceptibility gives the response of the system to a magnetic field which is the same in the two sublattices (note that we are neglecting the influence of the states where the states have zero weight of $\mathbf{k} = 0$), and induces a ferromagnetic ordering. The antisymmetric response leads to antiferromagnetic ordering. The susceptibilities can be written as:

$$\begin{aligned} \chi_D(\mathbf{q};!) &= \frac{t_2}{4} \int_0^{2\pi} \int_0^{2\pi} k dk \frac{d}{2} \frac{1}{1 - t_2 \frac{\cos^2(k+q=2)}{k+q=2} \frac{1}{k-q=2}} \frac{1}{1 - t_2 \frac{\cos^2(k+q=2)}{k+q=2} \frac{1}{k-q=2}}; \\ \chi_{ND}(\mathbf{q};!) &= \frac{t_2}{4} \int_0^{2\pi} \int_0^{2\pi} k dk \frac{d}{2} \frac{\cos^2(k+q=2)}{1 - t_2 \frac{\cos^2(k+q=2)}{k+q=2} \frac{1}{k-q=2}} \frac{\cos^2(k+q=2)}{1 - t_2 \frac{\cos^2(k+q=2)}{k+q=2} \frac{1}{k-q=2}}; \end{aligned} \quad (16)$$

where $\theta_{k+q=2, k-q=2}$ is the angle between $\mathbf{k} + \mathbf{q}=2$ and $\mathbf{k} - \mathbf{q}=2$, and:

$$\cos^2 \theta_{k+q=2, k-q=2} = \frac{(\mathbf{k} + \mathbf{q}=2) \cdot (\mathbf{k} - \mathbf{q}=2)}{|\mathbf{k} + \mathbf{q}=2| |\mathbf{k} - \mathbf{q}=2|} = \frac{(k^2 - q^2)^2}{(k^2 + q^2)^2 - 4k^2 \cos^2(\theta)} \quad (17)$$

The only dependence on the angle θ between the vectors \mathbf{k} and \mathbf{q} of the expressions in Eq. (16) is (after using the double angle formula) through the cosine in Eq. (17). Averaging over angles, we obtain:

$$\cos^2 \theta_{k+q=2, k-q=2} = \frac{k^2 - q^2}{k^2 + q^2}; \quad (18)$$

Inserting this expression into Eq. (16) it is a simple task to perform the remaining one-dimensional integral. Introducing $\chi_{\text{FM}}^0 = \chi_D(\mathbf{q};!) + \chi_{ND}(\mathbf{q};!)$ and $\chi_{\text{AFM}}^0 = \chi_D(\mathbf{q};!) - \chi_{ND}(\mathbf{q};!)$ we can extract the leading dependence on the

cut-off of the susceptibilities, and we finally obtain:

$$\begin{aligned}
 \text{Re } \chi_{\text{FM}}^0(\mathbf{q};!) &= \frac{1}{4} \sum_{s=1}^X \frac{\hbar}{t_2} \ln \frac{\hbar^2}{\hbar^2=2} \frac{s! \hbar}{s! \hbar} + \frac{\hbar^2}{2s!} \ln \frac{2\hbar^2}{\hbar^2=2} \frac{s! \hbar}{s! \hbar} \frac{i}{s! \hbar}; \\
 \text{Re } \chi_{\text{AFM}}^0(\mathbf{q};!) &= \frac{t_2}{8} \sum_{s=1}^X \ln \frac{2^2}{\hbar^2=2} \frac{s! \hbar}{s! \hbar} \text{Re } \chi_{\text{FM}}^0(\mathbf{q};!); \\
 \text{Im } \chi_{\text{FM}}^0(\mathbf{q};!) &= \frac{t_2}{4} \sum_{j=1}^h \frac{\hbar^2}{2j! \hbar^2} \frac{j! \hbar}{2t_2} \frac{\hbar^2}{j! \hbar^2} \frac{j! \hbar}{t_2} \frac{i}{\text{sign}(!)}; \\
 \text{Im } \chi_{\text{AFM}}^0(\mathbf{q};!) &= \frac{t_2}{8} \sum_{j=1}^h \frac{j! \hbar}{2t_2} \text{sign}(!) \text{Im } \chi_{\text{FM}}^0(\mathbf{q};!); \quad (19)
 \end{aligned}$$

Hence, setting $q = 0$, the antiferromagnetic susceptibility diverges logarithmically with the cut-off for any finite frequency $!$. The logarithmic dependence implies the existence of an instability for any positive value of the interaction U . Alternatively, we can show the existence of this instability by a direct calculation of the correlation energy gained by polarizing the system.

It is worth noting that the divergence obtained here, and the related marginal behavior of a local interaction can be obtained from the same power counting arguments used for the analysis of two dimensional interacting electrons near a van Hove singularity¹⁹. If we include next nearest neighbor couplings through the parameter γ , as discussed in Section IV, the low energy bands can be described by an effective Dirac equation. The screening of the long range Coulomb interaction vanishes, and the corresponding susceptibility can also be calculated analytically^{20,21}.

Note also that the polarization function is simply related to the susceptibilities²² above by $\chi^0 = \chi^0$. This allows one to get the screening properties within the RPA easily. In particular, for the mode that is symmetric in the layer densities which originally had the long-wavelength $1=jj$ singularity the static ($! = 0$) RPA screening cuts off the singularity by taking $1=jj!$ $1=(jj+q_{\text{TF}})$. From Eq. (19) we find that the Thomas-Fermi screening wavevector q_{TF} / t_2 . This is in agreement with what one expects from the usual two-dimensional electron gas where the screening wave-vector is $/m$ independently of the density of carriers^{23,24}.

B. Mean-field approach

Alternatively we can explain the diverging susceptibility with a simple mean-field approach. We introduce a staggered mean-field into the Hamiltonian according to

$$K(\mathbf{p}) = \begin{pmatrix} 0 & pe^{i(\mathbf{p})} & t_2 & 0 & 1 \\ Bpe^{i(\mathbf{p})} & 0 & 0 & 0 & C \\ t_2 & 0 & 0 & pe^{i(\mathbf{p})} & A \\ 0 & 0 & pe^{i(\mathbf{p})} & 0 & 0 \end{pmatrix}; \quad (20)$$

where the label different spin orientations. The four bands are then:

$$\epsilon(k) = \frac{s}{2} \frac{2k^2 + t_2^2 + 2^2 \hbar^2}{\hbar^2} \sqrt{4k^2 + t_2^2}; \quad (21)$$

The opening of the gap lowers the kinetic energy of the system. We estimate this by performing the integral up to $k = \pi$, then for $t_2 = .05$

$$E_{\text{kin}} = 21.9043 \frac{t_2}{2} \ln(\pi) + O(\pi^3); \quad (22)$$

is the change in the kinetic energy per unit cell due to $!$. The connection between the average magnetization $M = \langle n_{j,\uparrow} \rangle - \langle n_{j,\downarrow} \rangle$ and the mean field is $U M = 2$, where U is the strength of the on-site Hubbard interaction. The energy price one must pay per unit cell for having doubly occupied sites is

$$E_U = U M^2 = \frac{4}{U} \hbar^2; \quad (23)$$

Because of the logarithm in Eq. (22) a small antiferromagnetic distortion is always favorable. Assuming that $!$ is small, the mean-field solution is:

$$M_{\text{MF}} = \exp \left(\frac{1}{2} \frac{2=U}{t_2=2} \right); \quad (24)$$

and hence $!$ is exponentially suppressed unless U is of the order of $!$. Other variations of the mean-field in Eq. (20) give similar results. Thus within the mean-field approximation, the antiferromagnetism found here is very weak unless the interaction is strong.

VI. CONCLUSIONS

In summary, we have shown that long-range Coulomb interactions in a clean graphene bilayer lead to a ground state that is magnetically polarized with electron and hole pockets. We have determined the phase diagram of this model as a function of the coupling strength and doping, with a first order phase transition line between the

paramagnetic and ferromagnetic states. Around the critical line one expects hysteresis effects associated with the presence of phase coexistence and/or magnetic domains. We have also shown that on-site electron-electron interactions produce a staggering of the ferromagnetic order in the two planes and hence, c-axis antiferromagnetism. The introduction of other terms in the Hamiltonian, such as trigonal distortions, makes the phase diagram even richer, due to the creation of new energy scales. It is clear from our studies that graphene bilayers present an electronic behavior that is rather different from ordinary metals. The study of these systems becomes even more relevant given the recent developments in the fabrication and control of graphene multi-layers, and their possible application in nano-electronics.

Acknowledgments

A.H.C.N. is supported through NSF grant DMR-0343790. F.G. acknowledges funding from MEC (Spain) through grant FIS2005-05478-C02-01, and the European Union contract 12881 (NEST).

APPENDIX A: UNITARY TRANSFORMATION

The unitary transformation M_p that one needs to diagonalize the Hamiltonian in Eq. (3) can be written as $M_p = M_1(p)M_2M_3(p)$, where

$$M_1(p) = \begin{pmatrix} 0 & 1 & 0 & 0 & 0 & 1 \\ 1 & 0 & 0 & 0 & 0 & 0 \\ 0 & 0 & e^{i(p)} & 0 & 0 & 0 \\ 0 & 0 & 0 & 1 & 0 & 0 \\ 0 & 0 & 0 & 0 & e^{i(p)} & 0 \end{pmatrix} \begin{matrix} C \\ A \\ C \\ A \\ C \\ A \end{matrix} \quad (A1)$$

is a gauge transformation,

$$M_2 = \frac{1}{2} \begin{pmatrix} 0 & 1 & 0 & 1 & 0 & 1 \\ 1 & 0 & 1 & 0 & 1 & 0 \\ 0 & 1 & 0 & 1 & 0 & 0 \\ 0 & 1 & 0 & 1 & 0 & 0 \end{pmatrix} \begin{matrix} C \\ A \\ C \\ A \\ C \\ A \end{matrix} \quad (A2)$$

forms symmetric/antisymmetric bands, and

$$M_3(p) = \begin{pmatrix} 0 & \cos[p(p)] & \sin[p(p)] & 0 & 0 & 1 \\ \sin[p(p)] & \cos[p(p)] & 0 & 0 & 0 & 0 \\ 0 & 0 & \cos[p(p)] & \sin[p(p)] & 0 & 0 \\ 0 & 0 & \sin[p(p)] & \cos[p(p)] & 0 & 0 \end{pmatrix} \begin{matrix} C \\ A \\ C \\ A \\ C \\ A \end{matrix}; \quad (A3)$$

takes care of the final diagonalizing rotation. Choosing $\tan[2p(p)] = 2p = t_2$ the rotated Hamiltonian $K_{diag}(p) = M_p^\dagger K(p) M_p$ becomes diagonal:

$$K_{diag}(p) = \text{diag} \quad \begin{matrix} t_2 = 2 - E(p); & t_2 = 2 + E(p); \\ t_2 = 2 + E(p); & t_2 = 2 - E(p) \end{matrix}; \quad (A4)$$

Except for the labeling of the states (A4), which is just a permutation, this is the unitary transformation we need to diagonalize the non-interacting problem.

APPENDIX B: EXCHANGE INTEGRAL FOR BLOCH ELECTRONS

Quite generally the Hartree-Fock energy consists of three terms. A kinetic term, a direct charging term, and an exchange term. The exchange term is²⁵

$$E_{ex} = \sum_{m,n} \sum_{j,j'} V_{m,n;j,j'} \langle m;n | j,j' | m;n \rangle; \quad (B1)$$

where V is the interaction potential and the sum is over occupied states. Expanding in Bloch states k_j we get

$$E_{ex} = \sum_{\substack{k_j; \\ k_0; 0}} \sum_{\substack{j \\ k_0; 0}} n_{k_j; j} n_{k_0; 0} J_{k_j k_0}^{j, 0}; \quad (B2)$$

where for the unscreened Coulomb interaction in 2D

$$J_{k_j k_0}^{j, 0} = \frac{e^2}{2} \int d^2x \int d^2x' \frac{w_{k_j}(x) w_{k_0; 0}(x) w_{k_0; 0}(x') w_{k_j}(x')}{j k x' j}: \quad (B3)$$

Let us consider one plane only, then we can write the Bloch states in the tight-binding approximation as

$$|k_j(x)\rangle = \sum_{T_A} e^{ik_j \cdot T_A} a_{k_j; w}(x - T_A) + \sum_{T_B} e^{ik_j \cdot T_B} b_{k_j; w}(x - T_B); \quad (B4)$$

where $w(x)$ is the localized basis function, T_A (T_B) are the lattice vectors of lattice A (B) and a_{k_j} and b_{k_j} are the functions that generate the Bloch state in question. Neglecting the overlap of wave-functions on the A and B sites we get approximately

$$|k_j(x)\rangle = |k_0; 0(x)\rangle e^{i(k_j - k_0) \cdot x} + |a_{k_j}; a_{k_0; 0}(x; k_j - k_0) + |b_{k_j}; b_{k_0; 0}(x; k_j - k_0): \quad (B5)$$

The functions a and b are periodic in the real-space lattice and can hence be expanded in components of harmonics of the reciprocal lattice k . Keeping only the leading constant term coming from the $K = 0$ terms we get $\delta = 1$, in which case

$$J_{k_j k_0}^{j, 0} = |a_{k_j}; a_{k_0; 0} + b_{k_j}; b_{k_0; 0}|^2 = |a_{k_0; 0} a_{k_j} + b_{k_0; 0} b_{k_j}|^2 \frac{2 e^2}{S j k - k_0^2}; \quad (B6)$$

The corrections to this $K = 0$ term are down by at least a factor of $j k - k_0^2$ as is explained in Ref. [25]. It is possible to include higher harmonics in the reciprocal lattice, but then the important divergence near $k = k_0$ is cut-off by $K \neq 0$. Moreover, including $K \neq 0$ we should also include

short-range (high energy) physics that is not described by the continuum model used here.

Note also that the expression in Eq. (B 6) is just what one gets from a simple Fourier transform if one also includes the spinor structure due to the two sub-lattices. We apply this to the bilayer where the Coulomb interaction can be written

$$H_I = \frac{1}{2} \sum_{\mathbf{r}} \sum_{\mathbf{r}'} \sum_{\mathbf{r}''} V^D(\mathbf{r} - \mathbf{r}') \psi_{\uparrow}(\mathbf{r}) \psi_{\downarrow}(\mathbf{r}') + \sum_{\mathbf{r}} \sum_{\mathbf{r}'} \sum_{\mathbf{r}''} V^{ND}(\mathbf{r} - \mathbf{r}') \psi_{\uparrow}(\mathbf{r}) \psi_{\downarrow}(\mathbf{r}') + \text{c.c.} \quad (\text{B } 7)$$

We Fourier transform this and introduce the symmetric and antisymmetric combinations

$$(\mathbf{q}) = \frac{1}{2} (\mathbf{q}) + \frac{1}{2} (\mathbf{q}) \quad (\text{B } 8)$$

to write the interaction in a diagonal form

$$H_I = \frac{1}{2S} \sum_{\mathbf{q}} \sum_{\mathbf{q}'} (\mathbf{q}) V(\mathbf{q}) (\mathbf{q}') \quad (\text{B } 9)$$

where $V = \frac{2e^2}{\epsilon_0 q} (1 - e^{iqd})/2$. The prime on the \mathbf{q} -sum denotes that the $\mathbf{q} = 0$ term should be excluded since it is canceled by the positive (jellium) background. In terms of the operators that diagonalizes the kinetic terms the density operators can be written as

$$(\mathbf{q}) = \sum_{\mathbf{p}} \sum_{\mathbf{p}+\mathbf{q}} \begin{pmatrix} \mathbf{p} + \mathbf{q}; \mathbf{p} \end{pmatrix} \quad (\text{B } 10)$$

where

$$\begin{pmatrix} \mathbf{p} + \mathbf{q}; \mathbf{p} \end{pmatrix} = \begin{pmatrix} \mathbf{p} + \mathbf{q} \\ \mathbf{p} \end{pmatrix} \begin{pmatrix} \mathbf{p} + \mathbf{q}; \mathbf{p} \end{pmatrix} \quad (\text{B } 11)$$

and $M_{\mathbf{p}}$ is given in Appendix A. Using this one can easily generalize Eq. (B 2) and (B 6) to arrive at Eq. (5).

APPENDIX C: EXCHANGE INTEGRAL

Using $V^D(\mathbf{q}) = 2 \frac{e^2}{\epsilon_0 q}$ and $V^{ND}(\mathbf{q}) = 2 \frac{e^2}{\epsilon_0 q} e^{iqd}$ one quite generally gets that the change in the exchange energy can be written as

$$\begin{aligned} \langle \frac{H_I}{2S} \rangle = & \frac{1}{2} \sum_{\mathbf{q}} \sum_{\mathbf{p}} \sum_{\mathbf{p}'} \frac{d\mathbf{p}}{(2\pi)^2} \frac{d\mathbf{p}'}{(2\pi)^2} \sum_{\mathbf{r}} \sum_{\mathbf{r}'} \sum_{\mathbf{r}''} V^D(\mathbf{r} - \mathbf{r}') \psi_{\uparrow}(\mathbf{r}) \psi_{\downarrow}(\mathbf{r}') + \sum_{\mathbf{r}} \sum_{\mathbf{r}'} \sum_{\mathbf{r}''} V^{ND}(\mathbf{r} - \mathbf{r}') \psi_{\uparrow}(\mathbf{r}) \psi_{\downarrow}(\mathbf{r}') + \text{c.c.} \quad (\text{C } 1) \end{aligned}$$

The K 's are sums of certain components of the matrices $\psi_{ij}(\mathbf{p}^0; \mathbf{p}) = \psi_{ij}(\mathbf{p}^0; \mathbf{p}) - \psi_{ji}(\mathbf{p}; \mathbf{p}^0)$. Note that the elements of ψ are all greater or equal to zero.

1. Half-filling

At half-filling the trial state is characterized by the single variational parameter Q . It is straightforward, albeit tedious, to perform the matrix multiplications and extract the K 's. The results for an electron and a hole pocket of size Q is:

$$K_1^D = \frac{p}{E(\mathbf{p})} \frac{p^0}{E(\mathbf{p}^0)} \cos(\theta_0); \quad (\text{C } 2)$$

$$K_1^{ND} = \frac{t}{2E(\mathbf{p}^0)} \left(1 - \frac{t}{E(\mathbf{p})} \right) \left(1 + \frac{t}{E(\mathbf{p})} \cos 2(\theta_0) \right); \quad (\text{C } 3)$$

$$K_2^D = \frac{1}{2} \frac{p}{E(\mathbf{p})} \frac{p^0}{E(\mathbf{p}^0)} \cos(\theta_0) + \frac{1}{2} \left(1 + \frac{t}{E(\mathbf{p})} \frac{t}{E(\mathbf{p}^0)} \right); \quad (\text{C } 4)$$

$$\begin{aligned} K_2^{ND} = & \frac{1}{2} \frac{p}{E(\mathbf{p})} \frac{p^0}{E(\mathbf{p}^0)} \cos(\theta_0) \\ & + \frac{1}{4} \left(1 - \frac{t}{E(\mathbf{p})} \right) \left(1 - \frac{t}{E(\mathbf{p}^0)} \right) \\ & + \left(1 + \frac{t}{E(\mathbf{p})} \right) \left(1 + \frac{t}{E(\mathbf{p}^0)} \cos 2(\theta_0) \right); \quad (\text{C } 5) \end{aligned}$$

In this appendix we temporarily relabel $t_2 = 2t$ to avoid an excessive amount of 2's in the equations. We can write

$$\langle \frac{H_I}{S} \rangle = \frac{g v_F^3}{4 \pi^2} C_1^D + C_1^{ND} + C_2^D + C_2^{ND}; \quad (\text{C } 6)$$

where we are measuring all parameters (i.e. Q and t) in units of the cut-off. The C 's are given by the integrals

$$\begin{aligned}
C_1^D &= 2Q^3 \int_0^1 \int_0^1 \int_0^1 dx dy dz \frac{x}{t^2 + (Qx)^2} \frac{y}{y^2 + t^2} \frac{\cos(n)}{y - Qxj} ; \\
C_1^{ND} &= Q^2 \int_0^1 \int_0^1 \int_0^1 dx dy dz \frac{t}{t^2 + y^2} \frac{e^{d \cdot y \cdot Qxjn}}{y - Qxj} \left(1 - \frac{t}{t^2 + (Qx)^2} \right) \left(1 + \frac{t}{t^2 + (Qx)^2} \right) \cos(2) ; \\
C_2^D &= \frac{Q^3}{2} \int_0^1 \int_0^1 \int_0^1 dx dy dz \frac{x}{t^2 + (Qx)^2} \frac{y}{t^2 + (Qy)^2} \cos(n) \\
&\quad + \left(1 + \frac{t}{t^2 + (Qy)^2} \right) \left(\frac{t}{t^2 + (Qx)^2} - \frac{1}{y - xj} \right) ; \\
C_2^{ND} &= \frac{Q^3}{4} \int_0^1 \int_0^1 \int_0^1 dx dy dz \frac{e^{d \cdot Q \cdot y \cdot xj}}{y - xj} 2Q^2 \frac{x}{t^2 + (Qx)^2} \frac{y}{t^2 + (Qy)^2} \cos(n) \\
&\quad + \left(1 - \frac{t}{t^2 + (Qx)^2} \right) \left(1 - \frac{t}{t^2 + (Qy)^2} \right) + \left(1 + \frac{t}{t^2 + (Qx)^2} \right) \left(1 + \frac{t}{t^2 + (Qy)^2} \right) \cos(2) ; \quad (C7)
\end{aligned}$$

From this one can extract the leading and sub-leading terms in an expansion in powers of Q , the result is given in Eq. (7). Some useful expressions for performing the expansion are provided in Appendix D.

2. Doped case

The calculation for the doped system proceeds exactly as in the previous case but we must allow for the electron and hole pockets to have different size. For each electron (or hole) pocket of size Q_e (Q_h) there is a contribution like that in Eq. (C1). The K 's are half of those in Eq. (C3), (C4) and (C5). But K_1^D is different for holes and electrons:

$$K_{1e=h}^D = \frac{1}{2} \frac{pp^0}{2E(p)E(p^0)} \cos(n); \quad (C8)$$

The contributions coming from the $l=2$ are easy to obtain and can be encoded in a new contribution C_{new} in Eq. (C6), where

$$C_{new} = Q^2 R_0(Q); \quad (C9)$$

and R_0 is given in Appendix D.

APPENDIX D: COULOMB INTEGRALS

Let us define

$$R_n(Q) = \int_0^1 \int_0^1 \int_0^1 dx dy dz \frac{xy \cos(n)}{Q^2 x^2 + y^2 - 2Qxy \cos(n)}; \quad (D1)$$

Then one can show that up to $O(Q^{10})$

$$\begin{aligned}
R_0(Q) &= \frac{h}{2} \left(1 - \frac{Q^2}{8} + \frac{Q^4}{64} - \frac{5Q^6}{1024} + \frac{35Q^8}{16384} \right); \\
R_1(Q) &= -\frac{Q}{6} \ln(Q) + \frac{1}{3} \ln(2) - \frac{1}{12} Q \\
&\quad - \frac{h}{2} \left(\frac{3Q^3}{80} + \frac{15Q^5}{1792} + \frac{175Q^7}{55296} + \frac{2205Q^9}{1441792} \right); \\
R_2(Q) &= \frac{2}{9} Q - \frac{h}{2} \left(\frac{3Q^2}{16} + \frac{5Q^4}{288} + \frac{21Q^6}{4096} + \frac{9Q^8}{4096} \right);
\end{aligned}$$

Moreover $R_0(1) = 4/3$, $R_1(1) = 2(2C - 1)/3$ and $R_2(1) = 4(3 - 7)/27$. $C = 0.91596$ is the Catalan constant.

APPENDIX E: APPROXIMATE TWO-BAND MODELS

There are two reasons for constructing approximate two-band models. Firstly, on physical grounds the high-energy bands should not be very important for the low-energy properties of the system. Secondly, it is much easier to work with 2 \times 2 matrices instead of 4 \times 4 matrices. In this appendix we derive the low-energy effective model by doing degenerate second order perturbation theory. The quality of the expansion is good as long as $v_F p \ll t_F$.

1. Simple low-energy model

If we transform the Hamiltonian matrix in Eq. (3) by taking the symmetric and anti-symmetric combinations of the first and third rows (and columns) we can write $H_{kin} = H_0 + H_1$, where

$$H_0 = \begin{pmatrix} 0 & t_F & 0 & 0 \\ 0 & 0 & 0 & 0 \\ 0 & 0 & t_F & 0 \\ 0 & 0 & 0 & 0 \end{pmatrix} \begin{pmatrix} 1 \\ 0 \\ 0 \\ 0 \end{pmatrix} \begin{pmatrix} 0 \\ 0 \\ 0 \\ 0 \end{pmatrix} \begin{pmatrix} 0 \\ 0 \\ 0 \\ 0 \end{pmatrix}; \quad (E1)$$

$$H_1 = \frac{1}{2} \begin{pmatrix} 0 & 0 & p e^{i(\varphi)} & 0 & p e^{i(\varphi)} \\ p e^{i(\varphi)} & 0 & 0 & p e^{i(\varphi)} & 0 \\ 0 & p e^{i(\varphi)} & 0 & 0 & p e^{i(\varphi)} \\ p e^{i(\varphi)} & 0 & p e^{i(\varphi)} & 0 & 0 \end{pmatrix} \begin{pmatrix} C \\ A \end{pmatrix} \quad (E2)$$

Performing second order perturbation theory one finds an effective Hamiltonian matrix, $H_e = H_1^Y (1 - H_0) H_1$, where:

$$H_e = \frac{p^2}{t_2} \begin{pmatrix} 0 & 0 & 0 & 0 & 1 \\ 0 & 0 & 0 & 0 & e^{2i(\varphi)} \\ 0 & 0 & 0 & 0 & 0 \\ 0 & 0 & 0 & 0 & 0 \\ 0 & e^{2i(\varphi)} & 0 & 0 & 0 \end{pmatrix} \begin{pmatrix} C \\ A \end{pmatrix} \quad (E3)$$

The low-energy spinors are then given by:

$$|\varphi\rangle = \frac{1}{2} \begin{pmatrix} 0 & 1 \\ 0 & 0 \\ e^{i(\varphi)} & 0 \end{pmatrix} \begin{pmatrix} C \\ A \end{pmatrix}; \quad (E4)$$

and the corresponding energies are $p^2 = t_2$. If we add the contribution from φ_3 (which is already diagonal in this basis) and only keep the B-atom components we immediately arrive at Eq. (10).

In fact it is easier to see the existence of the exchange instability in this basis. Working in this subspace we again get an expression like that in Eq. (C1) with $K_1^D = 0, K_1^{ND} = \cos(2)$, $K_2^D = 1$ and $K_2^{ND} = \cos(2)$. If one further neglects the difference between V^D and V^{ND} the resulting change in the exchange energy can be expressed with the help of the functions defined in Appendix D. Explicitly the leading term in the exchange energy is $\frac{1}{8Q^2} R_0(1) + R_2(1) + 2Q^2 R_2(Q) - 8Q^2 = 27$ in agreement with the result in Eq. (7).

2. More general low-energy model

A more general Hamiltonian model for the low energy physics is given by³:

$$H_0 = \begin{pmatrix} 0 & 0 & v_F p e^{i\varphi} & t_2 & v_4 p e^{i\varphi} \\ v_F p e^{i\varphi} & 0 & v_4 p e^{i\varphi} & v_3 p e^{i\varphi} & C \\ t_2 & v_4 p e^{i\varphi} & 0 & v_F p e^{i\varphi} & 0 \\ v_4 p e^{i\varphi} & v_3 p e^{i\varphi} & v_F p e^{i\varphi} & 0 & 0 \end{pmatrix} \begin{pmatrix} C \\ A \end{pmatrix} \quad (E5)$$

One can perform a unitary transformation so that $H_2 = M^{-1} H_0 M$, where $M = M_1(\varphi) M_2$ and $M_1(\varphi)$ and M_2 are given in Eq. (A1) and (A2). We may then separate the transformed Hamiltonian into three parts, $H_2 = K_0 + K_1 + K_2$, with:

$$K_0 = \begin{pmatrix} 0 & t_2 & 0 & 0 & 1 \\ t_2 & 0 & 0 & 0 & 0 \\ 0 & 0 & t_2 & 0 & 0 \\ 0 & 0 & 0 & 0 & 0 \end{pmatrix} \begin{pmatrix} C \\ A \end{pmatrix}; \quad (E6)$$

$$K_1 = \begin{pmatrix} 0 & 0 & 0 & 0 & 1 \\ 0 & v_3 p \cos(3) & 0 & i v_3 p \sin(3) & C \\ 0 & 0 & 0 & 0 & A \\ 0 & i v_3 p \sin(3) & 0 & v_3 p \cos(3) & 0 \end{pmatrix} \begin{pmatrix} C \\ A \end{pmatrix}; \quad (E7)$$

$$K_2 = \begin{pmatrix} 0 & 0 & (v_F + v_4)p & 0 & 0 \\ (v_F + v_4)p & 0 & 0 & 0 & 0 \\ 0 & 0 & 0 & 0 & (v_F - v_4)p \\ 0 & 0 & 0 & (v_F - v_4)p & 0 \end{pmatrix} \begin{pmatrix} C \\ A \end{pmatrix}; \quad (E8)$$

With this decomposition it is easy to find the approximate eigenstates and eigenvalues for $v_F p \ll t_2$.

For the high-energy states one can use the simple non-degenerate perturbation theory. The eigenvalues are given by $E_3 = t_2 + (v_F + v_4)^2 p^2 = t_2$ and $E_4 = t_2 - (v_F - v_4)^2 p^2 = t_2$. It is also straightforward to obtain the corresponding states. For the low-energy sector the second order perturbation result (from two K_2 and one K_0) can give a term which is of the same order as that of K_1 . Thus, we must use degenerate perturbation theory. The usual manipulations then given the Hamiltonian matrix in the low energy subspace as $K_{low} = K_1 - K_2 P_1 (1 - K_0) P_1 K_2$, where P_1 is the projection out of the low-energy subspace, explicitly

$$K_{low} = \begin{pmatrix} 0 & 0 & 0 & 0 & 1 \\ 0 & v_3 p \cos(3) & 0 & i v_3 p \sin(3) & C \\ 0 & 0 & 0 & 0 & A \\ 0 & i v_3 p \sin(3) & 0 & v_3 p \cos(3) & 0 \end{pmatrix} + \frac{p^2}{t_2} \begin{pmatrix} 0 & 0 & 0 & 0 & 1 \\ 0 & (v_F + v_4)^2 & 0 & 0 & 0 \\ 0 & 0 & 0 & 0 & 0 \\ 0 & 0 & 0 & (v_F - v_4)^2 & 0 \end{pmatrix} \begin{pmatrix} C \\ A \end{pmatrix}; \quad (E9)$$

and the corresponding eigenvalues are

$$E = \frac{2v_F v_4 p^2}{t_2} \pm \frac{h}{(v_3 p)^2 + \frac{h}{t_2} (v_F^2 + v_4^2) p^2} \frac{h}{2(v_3 p)} \frac{(v_F^2 + v_4^2) p^2}{t_2} \cos(3): \quad (E10)$$

¹ K. S. Novoselov, A. K. Geim, S. V. Morozov, D. Jiang, M. I. Katsnelson, I. V. Grigorieva, S. V. Dubonos, and

A. A. Firsov, Nature 438, 197 (2005).

- ² Y. Zhang, Y.-W. Tan, H. L. Stormer, and P. Kim, *Nature* 438, 201 (2005).
- ³ P. R. Wallace, *Phys. Rev.* 71, 622 (1947).
- ⁴ N. M. R. Peres, F. Guinea, and A. H. Castro Neto, *cond-mat/0506709*.
- ⁵ N. M. R. Peres, F. Guinea, and A. H. Castro Neto, *Phys. Rev. B* 73, 125411 (2006).
- ⁶ N. B. Brandt, S. M. Chudinov, and Y. G. Ponomarev, in *Modern Problems in Condensed Matter Sciences*, edited by V. M. Agranovich and A. A. Maradudin (North Holland (Amsterdam), 1988), vol. 20.1.
- ⁷ H. Rydberg, M. Dion, N. Jacobson, E. Schroder, P. Hyldgaard, S. Simak, D. Langreth, and B. Lundqvist, *Phys. Rev. Lett.* 91, 126402 (2003).
- ⁸ P. Esquinazi, D. Spemann, R. Hohné, A. Setzer, K.-H. Han, and T. Butz, *Phys. Rev. Lett.* 91, 227201 (2003).
- ⁹ M. A. H. Vozmediano, M. P. Lopez-Sancho, T. Stauber, and F. Guinea, *Phys. Rev. B* 72, 155121 (2005).
- ¹⁰ N. M. R. Peres, F. Guinea, and A. H. Castro Neto, *Phys. Rev. B* 72, 174406 (2005).
- ¹¹ F. Bloch, *Z. Physik* 57, 549 (1929).
- ¹² C. Berger, Z. Song, T. Li, X. Li, A. Y. Ogbazghi, R. Feng, Z. Dai, A. N. M. Archenkov, E. H. Conrad, P. N. First, et al., *J. Phys. Chem.* 108, 19912 (2004).
- ¹³ F. Guinea, G. Gomez-Santos, and D. Arovas, *Phys. Rev. B* 62, 391 (2000).
- ¹⁴ X. Du, S.-W. Tsai, D. L. Maslov, and A. F. Hebard, *Phys. Rev. Lett.* 94, 166601 (2005).
- ¹⁵ J. W. McClure, *Phys. Rev.* 108, 612 (1957).
- ¹⁶ J. C. Slonczewski and P. R. Weiss, *Phys. Rev.* 109, 272 (1958).
- ¹⁷ E. McCann and V. I. Fal'ko, *Phys. Rev. Lett.* 96, 086805 (2006).
- ¹⁸ N. M. R. Peres, M. A. N. Araújo, and D. Bozi, *Phys. Rev. B* 70, 195122 (2004).
- ¹⁹ J. Gonzalez, F. Guinea, and M. A. H. Vozmediano, *Nucl. Phys. B* 485 [FS], 694 (1997).
- ²⁰ J. Gonzalez, F. Guinea, and M. A. H. Vozmediano, *Nucl. Phys. B* 424 [FS], 595 (1994).
- ²¹ J. Gonzalez, F. Guinea, and M. A. H. Vozmediano, *Phys. Rev. Lett.* 77, 3589 (1996).
- ²² G. D. Mahan, *Many-Particle Physics* (Plenum, 2000).
- ²³ E. Canel, M. P. Matthews, and R. K. P. Zia, *Phys. kondens. Materie* 15, 191 (1972).
- ²⁴ A. L. Fetter, *Ann. Phys.* 81, 367 (1973).
- ²⁵ C. Herring, *Magnetism*, vol. 4 (Academic Press, New York, 1966).